교육학 석사 학위논문

Optically Tunable Bumpy Silver Nanoshells with Size-varied Silica Cores: Synthesis and their Surface Enhanced Raman Scattering Characteristics

실리카 코어 크기 조절을 통하여 광학적 가변성을 갖는 범피 실버 나노쉘의 합성과 표면 증강 라만 산란 특성에 대한 연구

2016 년 8 월

서 울 대 학 교 대 학 원

과학교육과 화학전공

고 은 별

Optically Tunable Bumpy Silver Nanoshells with Size-varied Silica Cores: Synthesis and their Surface Enhanced Raman Scattering Characteristics

지도교수 정 대 홍

이 논문을 교육학 석사 학위논문으로 제출함

2016 년 8 월

서울대학교 대학원

과학교육과 화학전공

고 은 별

고은별의 교육학석사 학위논문을 인준함

2016 년 8 월

위 원 장 _____ (인)

부위원장 _____ (인)

위 원 _____ (인)

Abstract

Optically Tunable Bumpy Silver Nanoshells with Size-varied Silica Cores: Synthesis and their Surface Enhanced Raman Scattering Characteristics

Eunbyeol Ko

Department of Science Education

(Major in Chemistry)

The Graduate School

Seoul National University

As SERS substrate, noble metal nanostructures on silica core template have been reported by many research groups taking advantages of chemical

stability due to silica core. However, as the size of silica core reduces, this benefit is no longer effective. This study reports successful fabrication of silver nanoshells on the amorphous silica nanoparticles (Si NPs) with different core size (59, 82, 103, 124, and 148 nm) by overcoming the increased instability on aggregation during fabrication with a decrease of core size. The problem coming from instability of the small Si NP core in the fabrication processes could be overcome by controlling the kinds of reducing agent, the amount of dispersing agent and the concentration of Si NPs. We obtained localized surface plasmon resonance (LSPR) and SERS spectra from the different sized AgNSs to analyze their size dependent optical properties. AgNSs in all sizes showed broad extinction from the visible to the near infrared (NIR) region, resulting in high SERS enhancement under three different excitation lasers (532, 660, and 785 nm). We introduced the concept of surface roughness as a factor of SERS enhancement in analysis of AgNS, and observed the correlation between the roughness of AgNS and SERS activities. Therefore, these results provide an understanding of size dependent SERS activity for AgNS achieving a base to use and select appropriate AgNS with different sizes depending on the purpose of research.

Key words: Silver nanoshell (AgNS), surface-enhanced Raman scattering (SERS), localized surface plasmon resonance (LSPR), optical tunability.

Student number: 2014-20960

Contents

List of Figures

List of Tables

1. Introduction

Surface enhanced Raman scattering (SERS) technique has been actively studied for diverse fields ranging from such as chemical,[1-4] physical[5-6] and biological[7-10] detection due to the outstanding detection sensitivity at the single molecule level[3, 11] and the narrow bandwidth[10]. By the way, SERS enhancement is certainly required for application with prominent performance.[12] SERS enhancement depends on nanoparticle plasmonic resonance, which provides localized electric field to amplify the Raman signals of target molecules.[13] It is well known that the degree of SERS enhancement highly relies on the plasmonic properties of nanostructure, which is determined mainly by the structure parameters of nanoparticles such as size and shape.[14-16] Therefore, preparing suitable SERS nanostructure is central concern for these various SERS applications.

Although various designs of SERS substrates have been developed,[17-20] the serious study of the size factors affecting the SERS activity has well not been performed so far.[14, 16, 21] Considering that excitation of surface plasmon is dependent on size of metallic nanostructures and optimal size is different in purpose of research, [22-25] preparing suitable size of nanoparticle is important for diverse application of SERS technique. Therefore, obtaining various sized nanoparticle library is worthwhile for providing enough candidates to select specific size of nanoparticle according to purpose and understanding of size effect on optical characteristics using the library

would be beneficial for extending SERS studies. The size effect on SERS study performed before employed single wavelength excitation or measured in colloidal solutions, which results in different outcome depending on the experimental conditions.[14, 16, 21, 26-27] The reliable and systematic investigation demands several exciting laser lines and could be obtained from single nanoparticle detection.[28-29] This problem can be overcome by using the distinguishable properties of bumpy silver nanoshell (AgNS) structure studied in our previous study.[30]

In our previous study, we reported that bumpy silver nanoshells (AgNSs) which consist of a silica nanoparticle (Si NP) core coated with a few tens of nanometers of silver as highly sensitive SERS substrate.[30] First, this structure has a merit of facile synthesis for seedless, one step synthetic route. Second, AgNS shows more prominent SERS characteristics compared to smooth metal shell. This structure was founded to exhibit highly amplified Raman signals, which is contributed by concentration of electromagnetic field at the edge of bumpy surface. [31-33] In addition, AgNSs provided broad absorption band owing to their bumpy structure, which could be applied to SERS technology effectively at universal wavelengths. Consequently, we could control the size of AgNS easily and find the size effect on SERS profile under universal exciting laser line at single nanoparticle level by using AgNS structure.

In this study, we extended previous studies of AgNS with a focus on demonstrating the size dependent optical characteristics. We studied the fabrication method of different sized AgNSs. And also LSPR and SERS profiles were explored for AgNS with different sizes. All these AgNSs exhibited broad extinction bands over the range of 350 − 800 nm regardless of the particle size, exhibiting high Raman enhancement under three different lasers (532, 660, and 785 nm). Also, the detailed SERS activities were analyzed depending on the size at single particle level. Finally, the roughness of AgNS with different size was defined and calculated for obtaining the insights for understanding AgNS size-dependent SERS activity.

2. Experimental Section

2.1 Meterials Tetraethyl orthosilicate (TEOS), Triton™ X-100 (for molecular biology), cyclohexane (anhydrous, 99.5%), 1-hexanol (reagent grade, 98%), 3-mercaptopropyl trimethoxysilane (MPTS), ethylene glycol (EG, spectrophotometric grade, ≥99%), silver nitrate ($AgNO_3$, 99.99%), polyvinylpyrrolidone (PVP, average M.W. 40,000), ammonium hydroxide (NH_4OH, 28-30%), ethanolamine (EA), and 4-fluorothiophenol (4-FBT) were obtained from Sigma-Aldrich (St. Louis, MO, USA). Absolute ethanol (99.9%) and anhydrous ethanol (99%) were purchased from Daejung (Busan, Korea). All the chemicals were used without further purification.

2.2 Synthesis of silica core nanoparticles with different size The Si NPs of *ca* 100 nm diameter or less were synthesized by the reverse micelle method.[34-35] Various amount of Triton-X, and 1-hexanol were dissolved in 7.7 mL of cyclohexane, and 350 μL of deionized water was added to the mixture. The resulting mixture was stirred at 700 rpm for 10 min. Then, the water micelles were formed in oil phase. Various amount of aqueous ammonium hydroxide (28-30%) and tetraethyl orthosilicate (TEOS, 50 μL) were added to the mixture. The reaction was continued for 20 h while the mixture was vigorously stirred at room temperature. The synthesized silica nanoparticles (Si NPs) were centrifuged and then washed with ethanol several times to remove the excess reagents. The size of Si NPs obtained was estimated to be 42, 59, 82, and 103 nm in diameter. The detail condition

used in the synthesis are summarized in Table 1.

The Si NPs that are larger than 100 nm were synthesized by the Stober method.[36] Tetraethyl orthosilicate (TEOS, 1.6 mL) was dissolved in 40 mL of absolute ethanol, and a 2.8 mL (124 nm sized Si NP) or 3.0 mL (148 nm sized Si NP) of aqueous ammonium hydroxide (28-30%) was added to the mixture. The resulting mixture was stirred for 20 h at room temperature. The synthesized silica nanoparticles (Si NPs) were centrifuged and then washed with ethanol several times to remove the excess reagents.

2.3 Synthesis of bumpy silver nanosells with different size (AgNSs)

The size-varied Si NPs were dispersed in 1 mL of ethanol solutions containing 50 μL of MPTS and 10 μL of aqueous ammonium hydroxide (28-30%) for functionalization with thiol groups. The mixtures were stirred for 6 h at 25 ℃, and the resulting MPTS-treated silica NPs were centrifuged and re-dispersed in ethanol repeatedly. Various amounts by each size of MPTS-treated Si NPs were dispersed in 25 mL aliquots of ethylene glycol containing 5 mg of PVP, after which 25 mL of an $AgNO_3$ solution (to a final $AgNO_3$ concentration of 3.5 mM) was added to the silica dispersion and vigorously mixed. A 19.50 μL aliquot of ethanolamine (5 mM) was then rapidly added into the silica dispersion in the case of the smaller silica NPs (42, 59, 82, and 103 nm), and a 41.2 μL aliquot of octylamine (5 mM) was then rapidly added into the silica dispersion in the case of the larger NPs (124, and 148 nm). Then, the resulting mixtures were stirred for 1 h at 25 ℃,

and then, centrifuged and washed with ethanol several times for purification. The amounts of MPTS-treated silica NPs used for reaction by each size are shown in the table 2.

2.4 Adsorption of Raman chemical on AgNSs First, the 5.0×10^{10} particles of AgNSs in each size were transferred to the 4-fluorebenzenethiol solutions (2 mM in ethanol). The resulting dispersions were shaken for 1 h at room temperature, and then centrifuged and washed with ethanol several times. In order to avoid the aggregation of Ag NSs, their surface was treated with PVP. A 1 mL portion of PVP (0.025 mM in ethanol) was mixed with 5.0×10^{10} particles of Ag NSs bearing Raman labels for 30 min, followed by centrifugation several times and resuspension in DI water.

2.5 Characterization UV-Visible extinction spectra of various sized Ag NSs were measured using an UV-Visible spectrometer (Cary 300, Varian, USA). The size, morphology and homogeneity of the Ag NSs were analyzed using a SEM instrument (SUPRA 55VP, Carl Zeiss) and TEM instrument (JEM1010, JEOL). The SERS spectra of the Ag NSs were obtained using a confocal microscope Raman system (LabRam 300, JY-Horiba) equipped with an optical microscope (BX41, Olympus). Raman scattering lights were collected in a back-scattering geometry and detected using a spectrometer equipped with a thermoelectrically cooled (-70 ℃) CCD detector. SERS signals from the samples in capillary were collected using a ×10 objective lens (NA 0.25) with three different laser lines (532, 660, and 785 nm). For

single particle SERS measurement, the samples were dropped on a patterned slide glass, and SERS spectra were measured by point-by-point mapping with 1-μm step size. The mapping experiments were carried out using a ×100 objective lens (NA 0.90) with three different laser lines (532, 660, and 785 nm). After the SERS measurement, SEM images of the same area were obtained using field emission-scanning electron microscopy for single particle based analysis. The 20 particles of Ag NSs were analyzed for estimation of single-particle SERS activity in each size under different excitation wavelengths.

Size (nm)	Triton-X	1-Hexanol	Ammonia
42.0 ± 2.6	1.88 g	1.6 mL	100 μL
59.3 ± 3.9	1.88 g	1.6 mL	75 μL
82.0 ± 12.3	2.4 g	1.8 mL	100 μL
103.0 ± 12.0	1.88 g	1.6 mL	60 μL

Table 1. The detail condition used in the synthesis of various sized Si NPs. (mean±S.D., n=20)

(per reaction batch, 30 mg of $AgNO_3$)

Sample name	Si NP size (nm)	Relative Surface areas per unit mass to 147.9 nm Si NP	**Reacting mass of Si NP (mg)**	Reacting surface area of Si NP (cm^2)
-	42.0	3.73	**0.5**	320
Si NP **(i)**	59.3	2.51	**0.8**	320
Si NP **(ii)**	82.0	1.80	**1.1**	320
Si NP **(iii)**	103.0	1.44	**1.4**	320
Si NP **(iv)**	123.7	1.20	**1.7**	320
Si NP (v)	147.9	1	**2.0**	320

Table 2. Relative surface areas per unit mass is different according to Si NP size as fourth row of this table. Reacting surface area of Si NPs were controlled equally as 320 cm^2 by adjusting amount of silica nanoparticles.

3. Results and Discussion

3.1 Synthesis and characterization of bumpy silver nanoshells with different size

The fabrication of various sized AgNSs can be achieved by modifying the reported protocol.[30] In our previous study, AgNSs were synthesized through direct reduction of a silver nitrate on the thiol functionalized silica surface in the presence of octylamine. Octylamine plays a role as not only capping ligand but also reducing agent and, which might be responsible for the reduction of Ag^{+} ions to Ag^{0} to initiate the nucleation on the surface of silica cores and growth of the silver shells.[30, 37] In this basis, our synthetic strategy is modulating the final size of AgNS by tuning the size of the Si NP cores. For investigating the effect of the core sizes on synthetic results of AgNS by the polyol method, Si NPs with two different sizes around 40-nm and 170-nm were prepared first. And the same procedures as reported were tried to fabricating AgNSs using 40-nm and 170-nm sized Si NP. While AgNS using 170-nm sized Si NP (AgNS_C170) was well fabricated as expected, the fabrication of AgNS using 40-nm sized Si NP (AgNS_C40) under the same synthetic condition exhibited several problems (Figure 2a and b). In case of AgNS_C40, they were subject to aggregation to decrease the surface energy by reducing their surface area during the processes coating of reduced silver ion on Si NP surface.[38]

The problem coming from the poor stability of the small Si NP core in the fabrication processes could be overcome by controlling the kinds of alkylamines instead of octylamine, the amount of PVP and the concentration of Si NPs. AgNS_C40 could be fabricated properly after the optimization, and the TEM image of AgNS_C40 is shown in Figure 2c. Figure 2d shows the UV-Visible spectra of the AgNS_C170, AgNS_40 before and after optimization. AgNS_C40 before the optimization exhibited the absorption band near 470 nm because of aggregation of Si NP cores resulting in incomplete silver coating,[39] while the common feature of broad absorption spanning the NIR region exhibited in AgNS_C40 after the optimization and AgNS_C170.

Figure 3 represents optimized synthetic condition using 40-nm sized Si NP in detail. Several controlled experiment were performed for the optimization of the synthesis which are shown in the Supporting Information in detail (Figure 3). First, amount of Si NP is reduced, decreasing the reacting surface for avoiding aggregation of Si NP, and also increasing the relative amount of precursor (Ag^{+}) for complete formation of silver nanoshell. While the reduced amount of Si NP from 2 mg to 0.5 mg led successful fabrication of AgNS, however, using less than 0.5 mg amount of Si NP resulted in the thick layer of silver shell. Because excessive amount of $AgNO_3$ compared to Si NP caused for AgNP to overgrow on the surface of Si NP, the final size is much larger than core size. Consequently,

when we used less than 0.5 mg, using 40-nm sized Si NP core would be meaningless. Second, $AgNO_3$ is used same amount as condition using 170-nm Si NP. We tried to use less than 30 mg amount of $AgNO_3$ to prevent emerging excessive AgNPs in solution, but formation of silver nanoshell is rather incomplete. Third, the amount of PVP as a dispersing agent is increased from 5 mg to 10 mg to prevent aggregation and fabricate homogeneously. When more than 10 mg amount of PVP is used, fabrication of AgNS is similar to using 10 mg amount of PVP. Last, the kind of reducing agent is changed from octylamine to ethanol amine. Hydroxyl group of ethanol amine is electron withdrawing group. Amine group of ethanol amine is difficult to donate electrons to silver ion because of inductive effect of hydroxyl group. The size of AgNP assembled on silica core is smaller when using ethanol amine compared to using octylamine, because Ag^+ cannot reduce well to Ag^0 with ethanolamine.[40]

In order to obtain size-varied AgNSs library, we tried to synthesize various size of Si NP cores ranging from ~59 nm to ~148 nm. The Si NPs of different sizes were used as seeds for silver growth, and the gradual growth of silver on the prepared Si NP cores resulted in various sized AgNSs with bumpy morphology with optimized protocol. We have controlled the shell thickness to around ~30 nm for all the AgNSs. Because the concentration of silver nitrate is already excess in this protocol, the core particle concentrations were decreased to control the reacting surface area of Si NPs

equally when increasing the size of Si NPs (Table 2). In all cases, the AgNSs were well dispersed in solutions without aggregation (Figure 4b). As shown in the Figure 4c, the diameter of synthesized AgNSs increased as the sizes of Si NPs core increased. By varying the Si NP core size, we obtained homogenous AgNSs ranging from ~119 nm to ~207 nm. The detailed information of core and final size, and shell thickness are shown in table 3.

The plasmonic properties of the AgNS (I) ~ (V) were analyzed from obtaining the UV-vis spectra as shown in the figure 4d. In all cases, the additional absorption band appeared at ~ 410 nm which is inherent to the Ag dielectric properties independent of particle size. All AgNSs showed broad excitation over almost visible range (350-800 nm) regardless of particle sizes owing to their bumpy structure. It reveals that various sized AgNSs have potential to effective application of SERS technique at universal wavelength due to their broad excitation wavelength range. In addition, the AgNS (III)~(V) exhibited relatively high absorption in NIR region, whereas absorption of AgNS (I) and (II) slightly decreased at the longer wavelengths. For the increase in size of nanoparticles, besides dipole absorption, the excitation cress-section depends on higher order multiple modes which cause the plasmonic resonance shifts to longer wavelength and the broadened bandwidth.[41-42] Consequently, plasmonic resonance of AgNS could be tuned by controlling their size, because their LSPR modes varied by their size.

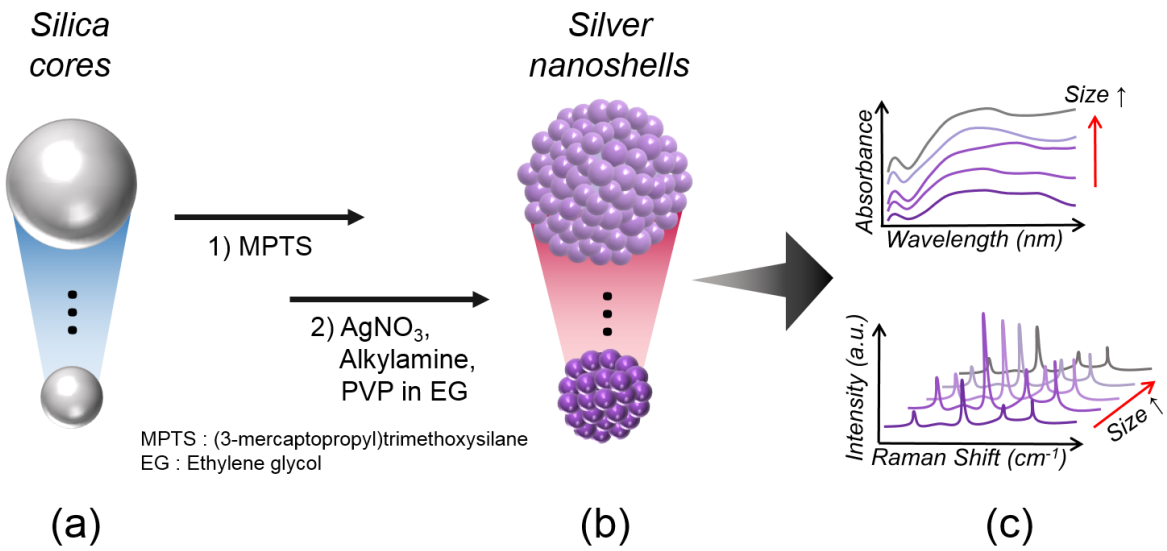

Figure 1. Schematic illustration for investigating the size-dependent optical properties using various sized AgNSs. Synthesis of (b) AgNSs with tunable sizes using (a) size-varied Si NP cores. (c) Analysis of the size-dependent optical properties of AgNS and SERS activities.

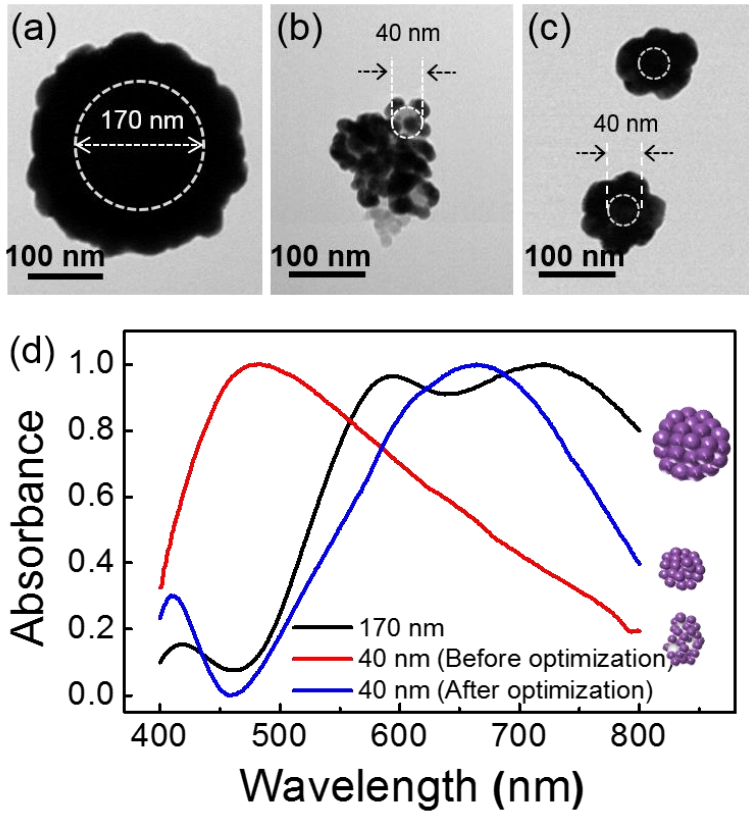

Fig 2. Comparison of synthesis of bumpy silver nanoshells (AgNSs) using different silica nanoparticles (Si NPs) with diameter of 170-nm and 40-nm as core particles. TEM images of synthesized AgNS with (a) 170-nm Si NP and (b) 40-nm Si NP under same synthetic conditions. (c) TEM images of AgNSs using 40-nm Si NP after optimizations (Fig. S2) (d) UV-Vis extinction spectra (normalized) of the AgNSs of (a)-(c).

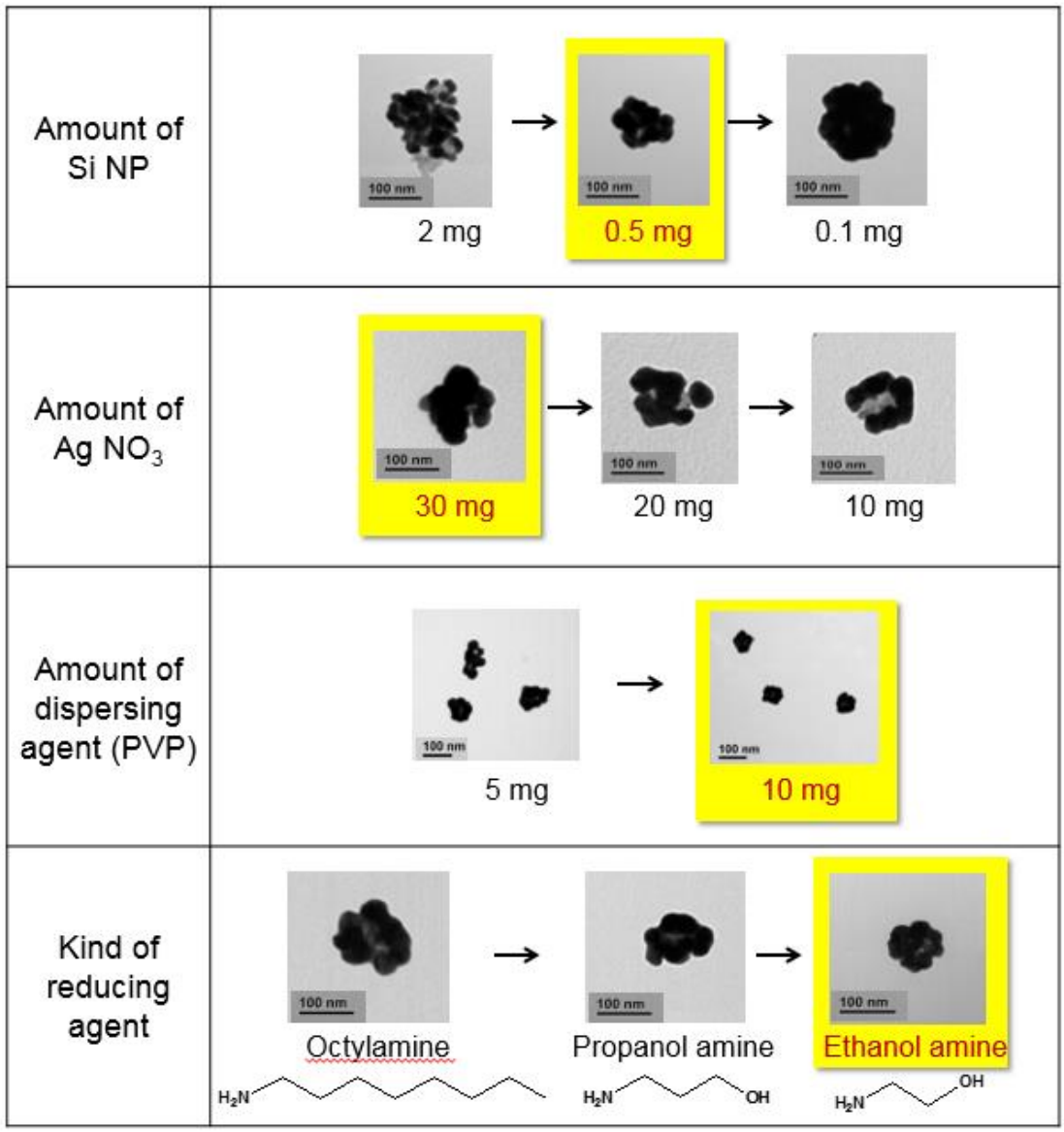

Fig 3. Optimization of synthesis of AgNS with 40-nm Si NP core. Classification of manipulated variables and TEM images of optimization processes. Yellow boxes indicate optimized synthetic conditions.

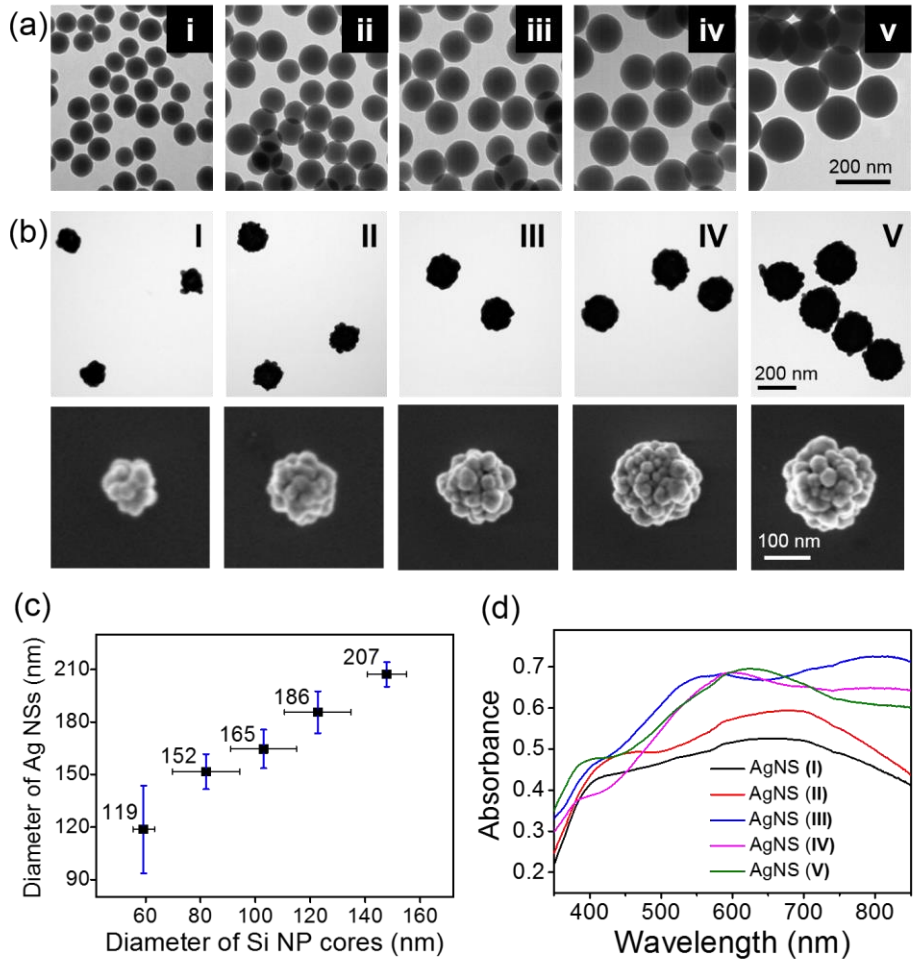

Fig 4. Synthesis of various sized silver nanoshells (AgNSs) using different size of silica nanoparticles (Si NPs). (a) TEM images of Si NPs with diameters of (i) 59 nm, (ii) 82 nm, (iii) 103 nm, (iv) 124 nm, and (v) 148 nm in average. (b) The TEM (upper panel) and SEM (lower panel) images of the synthesized AgNS **(I-V)** using the Si NPs of (a). (c) Correlation between diameter of the Si NP core **(i-v)** and that of the AgNS **(I-V)** (mean ± S.D., n = 20). (d) The absorption spectra of AgNSs **(I – V)**.

Sample name	Si NP core size (nm)	Final AgNS size (nm)	Thickness of Ag shell (nm)
AgNS **(I)**	59.3 ± 3.9	118.7 ± 25	29.7 ± 7
AgNS **(II)**	82.0 ± 12.3	151.6 ± 10	34.8 ± 4
AgNS **(III)**	103.0 ± 12.0	164.6 ± 11	30.8 ± 6
AgNS **(IV)**	123.7 ± 12.1	185.5 ± 12	31.4 ± 5
AgNS **(V)**	147.9 ± 7.1	207.2 ± 7	29.7 ± 5

Table 3. Detail structure of AgNSs by Si NP core size. (mean ± S.D., n = 20)

3.2 SERS analysis of different sized AgNSs

We also explored the SERS activity of the different sized AgNSs. Each AgNS samples was treated with 4-FBT, which chemisorbs on the silver shell surfaces. Due to the additional treatment with PVP, 4-FBT adsorbed AgNSs were well dispersed with no aggregating features in solution as shown in Figure 5. All the plots shown in the Figure 5 have an even distribution to the mode value of the particle size. To compare the SERS intensity depending on the size of AgNS and the excitation wavelength, the Raman spectra from AgNSs in the ethanol solution of same particle concentrations were measured, and normalized with a typical ethanol band ($882cm^{-1}$) under three different lasers (532, 660 and 785 nm) (Figure 6a). To investigate SERS effect per single molecule according to size of AgNS, peak intensities at 1075 cm^{-1} were normalized with surface area. (Figure 6b). The SERS activities decreased as the AgNS sizes increased regardless of laser excitation wavelength except the case of AgNS (I). Also, we examined SERS effect of AgNS according to excitation wavelength. SERS intensities increased as excitation wavelengths increased to NIR region in all size of AgNS. The result is consistent with previous report that AgNS is NIR-active substrate.[30]

To identify SERS activities of five different sized AgNSs at single particle level, single particle detection performed with three different lasers. The calculation of SERS enhancement factors (EF) from different sized AgNSs

demonstrated high SERS EFs from 6.4 X 10^5 to 2.2 X 10^7 at the three excitation wavelengths. We supposed that AgNSs have potential to effective application of SERS technique at universal wavelength based on absorption spectra data that all AgNSs showed broad excitation regardless of particle size as noted above. The SERS EF result proves experimentally that all sized AgNSs could be used for the SERS detections effectively for universal excitation wavelength. This highly sensitive SERS effect regardless of particle size resulted in by the bumpy structure of AgNSs that has strong E-field concentration.[30] In addition, we observed that SERS enhancement of single AgNS have similar tendencies to SERS activity of AgNS in solution and AgNS (II) exhibited the maximum enhancement among five sized samples (Figure 7c). This result from single particle detection might verify correlation between size and SERS enhancement more clearly. In order to obtain a better understanding on the size dependent SERS enhancement activities, we introduced roughness concept**.**

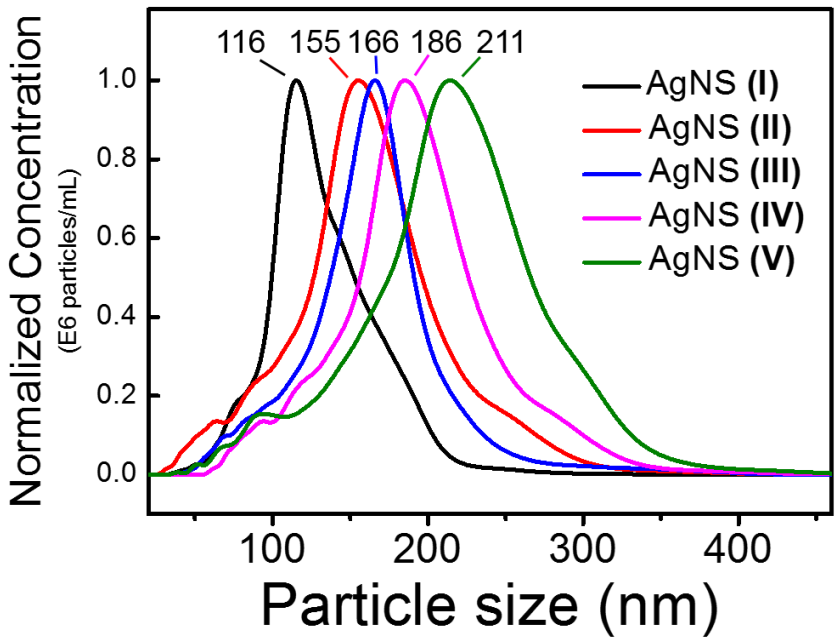

Fig 5. The sizes of AgNS (**I-V)** were analyzed by Nanoparticle Tracking Analysis (NTA). The plots represent particle size distribution of AgNS (**I-V)**. The numbers written above the plots correspond to mode of particle size I-V.

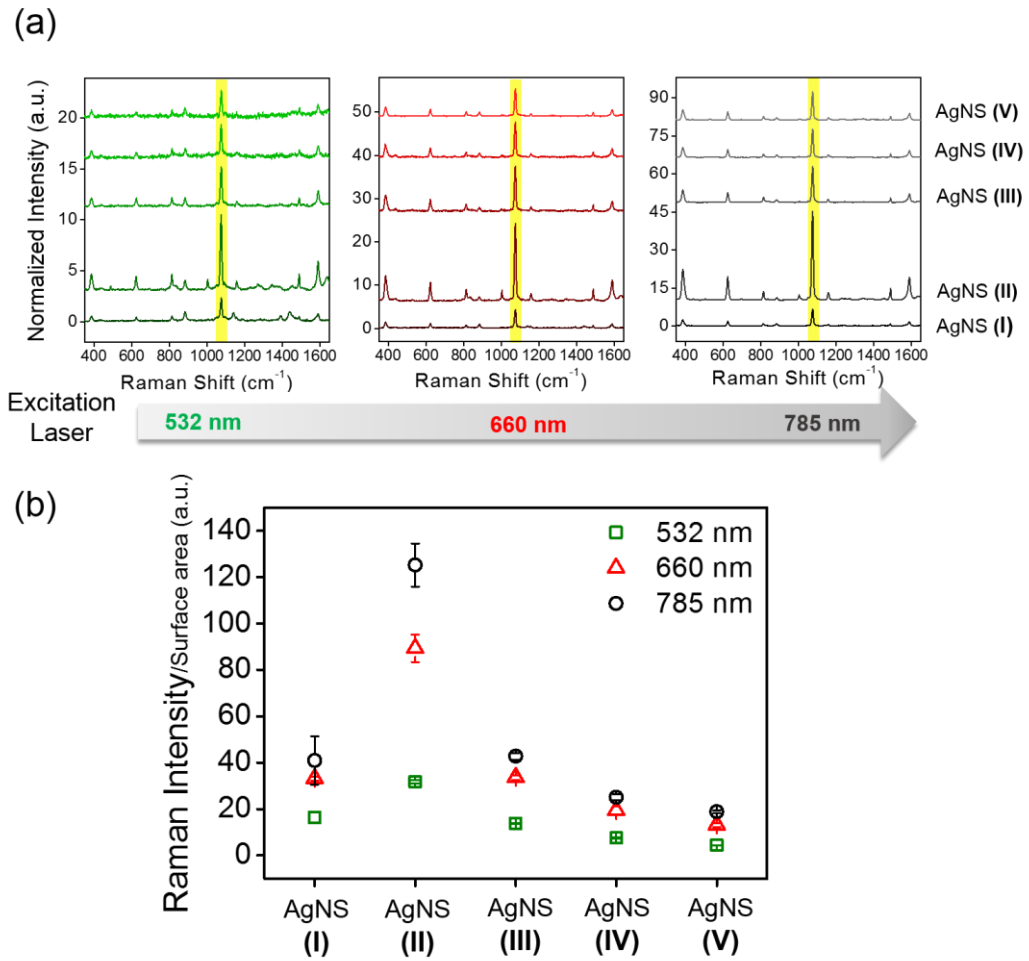

Fig 6. Analysis of SERS properties of AgNSs with different excitation lasers. (a) Normalized SERS spectra of 4-Fluorobenzenethiol (4-FBT) on every size of AgNSs (**I-V)** using three different excitation lasers of 532 nm (8.3 mW), 660 nm (6.6 mW), and 785 nm (10.0 mW). All spectra were obtained in ethanol by 1 s acquisition. (b) SERS intensities of the peak at 1075 cm^{-1} per relative surface area for the various sized Ag NSs **(I-V)** at three excitation wavelength (532, 660, and 785 nm).

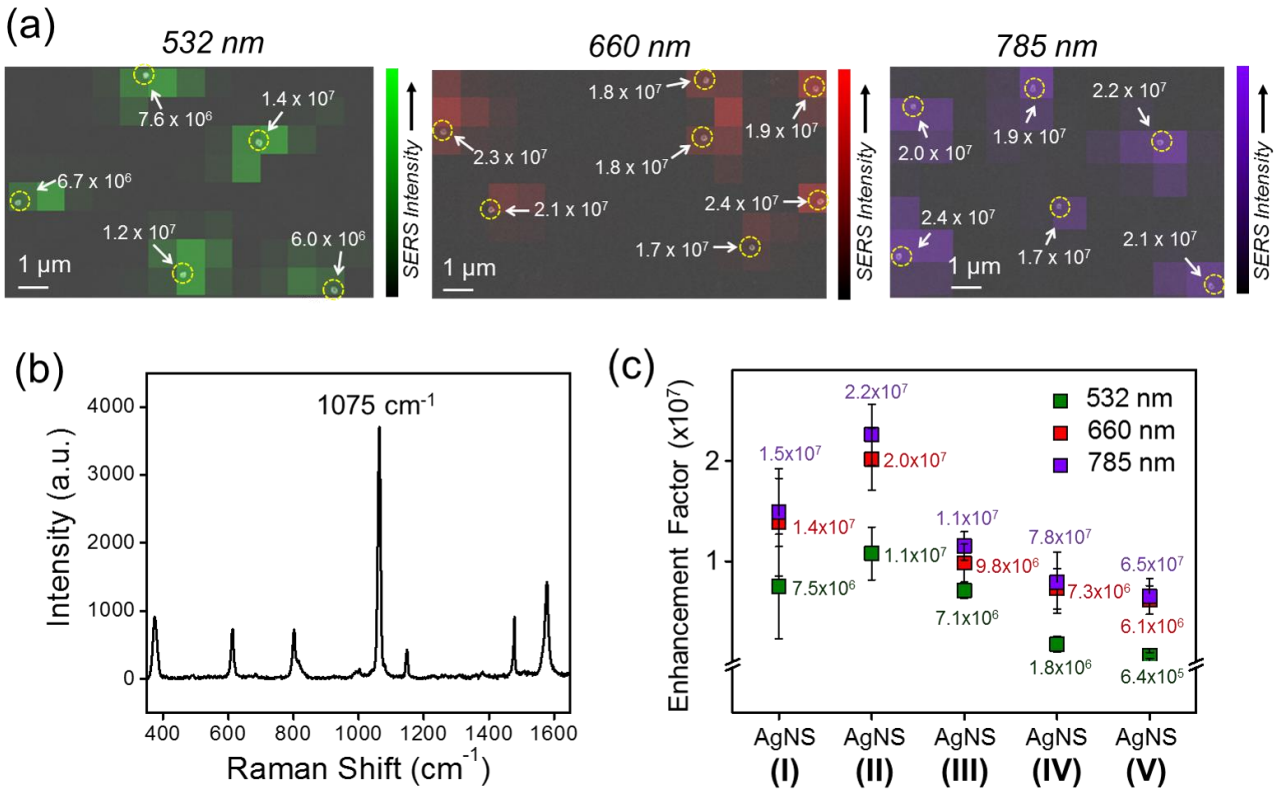

Fig 7. Single particle detection of different sized AgNSs. (a) SERS intensity map with enhancement factor values of a single AgNS **(II)** particle at the 1075 cm^{-1} of 4-FBT **;** the intensity map was overlaid with their corresponding SEM image. Scale bar is 1 µm. The upper/lower map is under 532, 660 and 785 nm photoexcitation. (b) SERS spectrum obtained from a single particle AgNS **(II)**$_{4\text{-FBT}}$ on the slide glass. The spectrum was taken with 532 nm photo-excitation (1.8 mW at the sample) and 2 s acquisition time. (c) Calculated enhancement factors of single AgNS **(I-V)** based on SERS intensity of 1075 cm^{-1} of 4-FBT.

3.3 Roughness parameters according to the size of AgNS

The size-dependent SERS enhancement of AgNS was analyzed in terms of the roughness of the silver shell surfaces. Roughened surface which produces an effective SERS active site due to strong concentration of electromagnetic field on the edge of surface could contribute to obtain high SERS enhancement effect.[43-46] AgNS is composed of silica NP as a core and Ag NPs assembled on the surface of silica core as a bumpy shell. The diameter of silver nanoparticles (Ag NP) assembled on silica core is similar in all sizes of AgNSs as ~30 nm based on Figure 8. If the sizes of particles attached to the core are same, we can predict that the roughness would increase as core size decreases. To confirm the roughness according to the size numerically, we created simple AgNS modeling and calculated roughness using the modeling.

We defined the roughness as an arithmetic average of deviation heights.[47-48] Figure 9a exhibits the method of calculating the roughness of AgNS graphically and numerically. For calculation of roughness factor, we defined mean line sphere (MLS) and the non-overlapping volume between MLS and AgNS was normalized by the surface of MLS. The sphere of equal volume with single AgNS is termed as mean line sphere (MLS). We can assess the roughness of individual AgNS using the equation : Roughness = $\frac{1}{A}\iint_A |Z(x,y)|\, dxdy$, where *A* is the surface of MLS and *Z (x,y)* is deviation height. So integral of |*Z(x,y)*| corresponds to the sum of deviation heights,

namely non-overlapping volume between MLS and AgNS. The sum of deviation heights (total volume above/below the MLS) was divided by the surface area of MLS (*A*) to calculate arithmetic average of deviation heights. The detail method and result of roughness measurement are represented in Figure 9b and Table 4. We can see that the roughness decreases from as the size of AgNS becomes larger as shown in Figure 10a. The roughness trend shows agreement with our assumption that the roughness would increase as core size decreases.

Figure 10b exhibits the dependency of the SERS intensity on the roughness parameter. The SERS intensity increased with the roughness factor, reaching a maximum with the roughness factor value of 3.51 AgNS (II). But AgNS (I) shows out of trend. AgNS (I) has poor stability compared to the other particles because of their small size. As shown in the Figure 11, size of the sample has a huge variation due to incomplete shell and aggregation of particles. So, AgNS (I) exhibits relatively low SERS intensity although roughness of AgNS (I) is the largest. The result indicates clear correlation between roughness and SERS intensity except AgNS (I). The main reason of roughness dependent SERS intensity of AgNS is that degree of conjunctions among bumps on their surface, termed as hot spots, would be varied by roughness, which is associated with SERS enhancement since hot spots can contribute to the localized electromagnetic mechanism.[49-51] Increase in the size of AgNS leads to a decrease in the

electromagnetic field at the hotspot and resultant decrease in the SERS intensity. Therefore, we demonstrated at the single particle level that size of AgNS is highly correlated with the SERS intensity in terms of their roughness. In this respect, this approach was considered to perform successfully for analysis of size-dependent SERS activities.

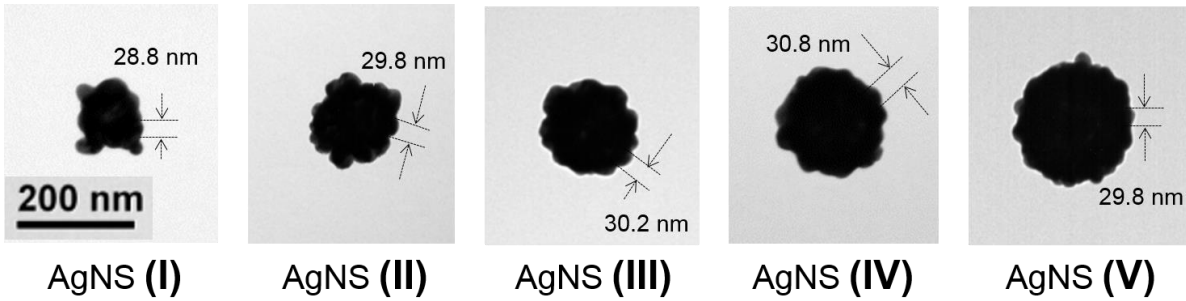

Fig 8. The two arrows in each TEM image indicate the size of Ag NP assembled on Si NP core. We measured 20 particles of Ag NPs and calculated the average size in each sample.

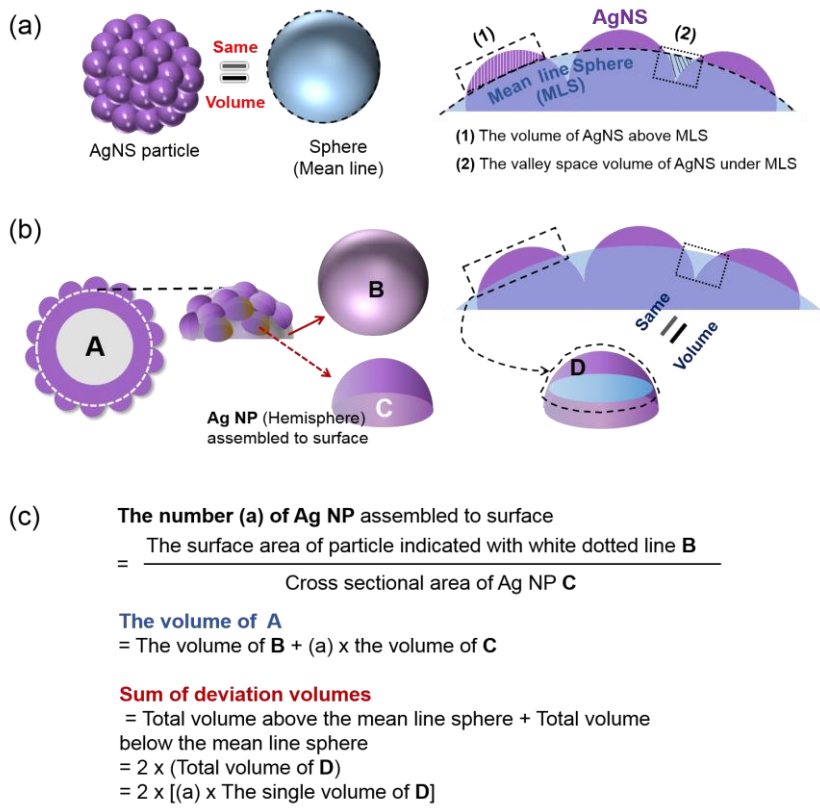

Fig 9. Roughness of AgNSs **(I-V).** (a) Illustration of nanoparticle modeling for representing roughness. The boxes with dashed/dotted line represent the volumes of AgNS above/below the mean line sphere. (b) Illustrations show the detailed modeling of bumpy AgNSs. The particle **A** is composed of a sphere **B** and several hemispheres **C** assembled to surface of **B. D** in the dotted box indicates the volume of AgNS above the mean line sphere**.** Total volume of **D** is same as the total volume of AgNS below the mean line sphere. (c) The calculating method of the volume of **A** and deviation volumes using modeling of (b).

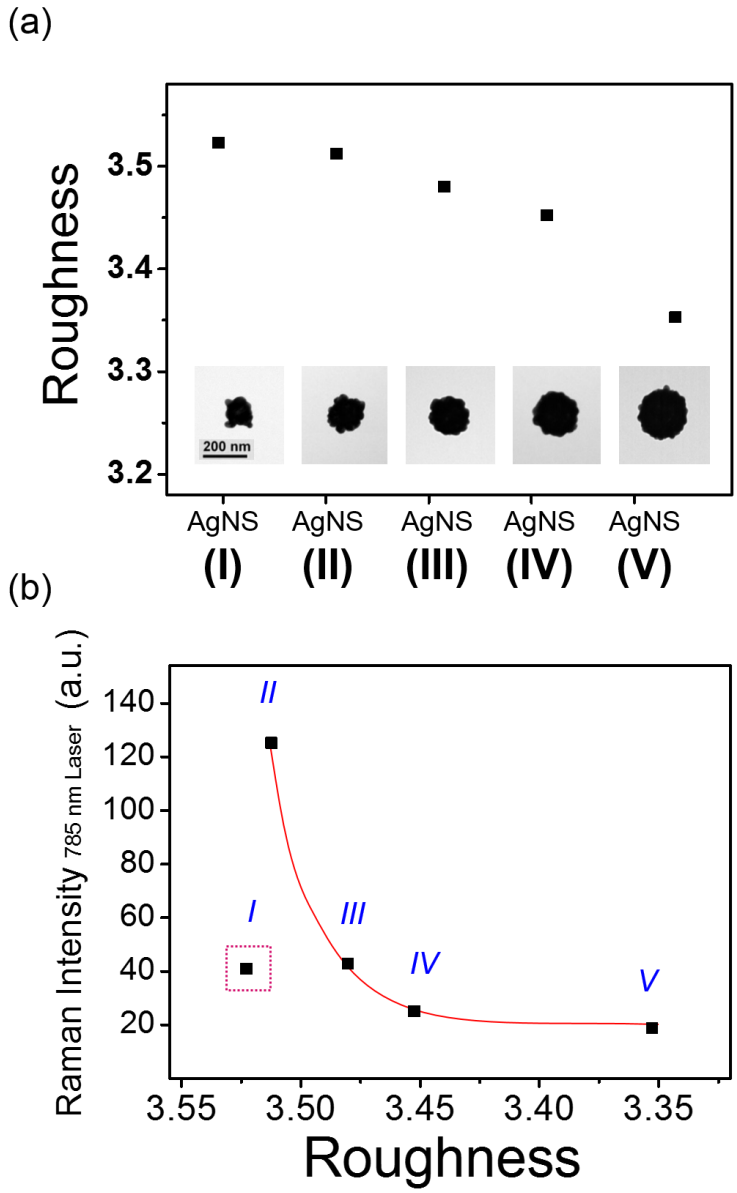

Fig 10. (a) Correlation between particle size and roughness of the particle. (b) Correlation between the roughness and Raman intensity (785 nm laser).

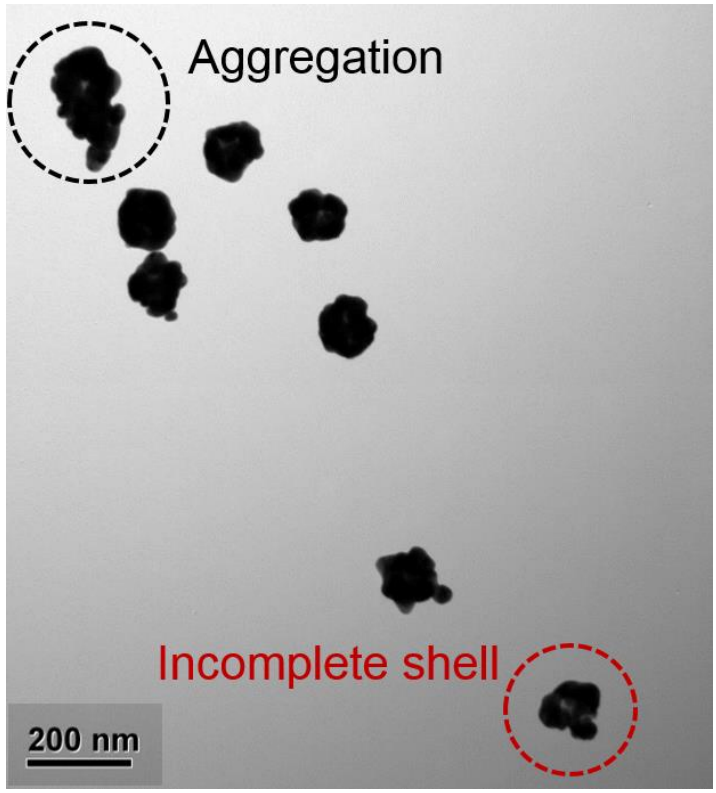

Fig 11. The TEM image of AgNS **I**. Black dotted circle indicates aggregation of particles. Red dotted circle indicates incomplete shell of particles. Because of the small size, AgNS **I** has relatively unstable structure compared to the other sized particles.

Sample name	Size of Ag NP assembled on Si NP core (nm)	Volume of AgNSs (nm^3)	Surface area of mean line sphere (nm^2)	Total deviation volume (nm^3)	Roughness
AgNS **(I)**	**29.6**	616446.20	35027.91	123397.46	**3.52**
AgNS **(II)**	**30.2**	1402910.21	60604.38	212864.06	**3.51**
AgNS **(III)**	**30.2**	1879527.30	73651.77	256323.05	**3.48**
AgNS **(IV)**	**30.3**	2721657.66	94269.92	325464.04	**3.45**
AgNS **(V)**	**29.8**	3905298.18	119927.91	402098.70	**3.35**

Table 4. Size of Ag NP assembled on Si NP core and calculation of roughness elements from bumpy Ag NS particles. (mean±S.D., n = 20)

4. Conclusion

In summary, we demonstrated an effective strategy for the size dependent SERS characteristics of bumpy silver nanoshells (AgNSs). Monodisperse AgNSs were developed with well controlled sizes by optimizing synthetic conditions. The diameter of AgNSs was finely tuned from ~119 nm to ~207 nm, changing their core size of silica. All these particles were used for SERS substrates, so we could identify their SERS enhancement with three different lasers (532, 660, 785 nm). It reveals that SERS efficiency is dependent on their sizes and the optimal size of AgNSs for which the SERS signal is maximized was obtained through investigation of the correlation between particle roughness and SERS enhancement. Thus, the results obtained this study could provide a base to use and select appropriate AgNSs with different sizes depending on the purpose of research.

5. References

1. Schlücker, S., Surface-Enhanced raman spectroscopy: Concepts and chemical applications. *Angew. Chem. Int. Ed.* **2014,** *53* (19), 4756-4795.
2. Dasary, S. S.; Singh, A. K.; Senapati, D.; Yu, H.; Ray, P. C., Gold nanoparticle based label-free SERS probe for ultrasensitive and selective detection of trinitrotoluene. *Journal of the American Chemical Society* **2009,** *131* (38), 13806-13812.
3. Kneipp, K.; Wang, Y.; Kneipp, H.; Perelman, L. T.; Itzkan, I.; Dasari, R. R.; Feld, M. S., Single molecule detection using surface-enhanced Raman scattering (SERS). *Phys. Rev. Lett.* **1997,** *78* (9), 1667.
4. Smith, W., Practical understanding and use of surface enhanced Raman scattering/surface enhanced resonance Raman scattering in chemical and biological analysis. *Chem. Soc. Rev.* **2008,** *37* (5), 955-964.
5. Schatz, G. C.; Young, M. A.; Van Duyne, R. P., Electromagnetic mechanism of SERS. In *Surface-enhanced Raman scattering*, Springer: **2006**, pp 19-45.
6. Tian, Z.-Q.; Ren, B., Adsorption and reaction at electrochemical interfaces as probed by surface-enhanced Raman spectroscopy. *Annu. Rev. Phys. Chem.* **2004,** *55*, 197-229.
7. Chang, H.; Kang, H.; Ko, E.; Jun, B.-H.; Lee, H.-Y.; Lee, Y.-S.; Jeong, D. H., PSA Detection with Femtomolar Sensitivity and a Broad Dynamic Range Using SERS Nanoprobes and an Area-scanning Method. *ACS Sensors* **2016**.
8. Huang, P. J.; Tay, L. L.; Tanha, J.; Ryan, S.; Chau, L. K., Single-Domain Antibody-Conjugated Nanoaggregate-Embedded Beads for Targeted Detection of Pathogenic Bacteria. *Chemistry–A European Journal* **2009,** *15* (37), 9330-9334.
9. Saha, K.; Agasti, S. S.; Kim, C.; Li, X.; Rotello, V. M., Gold nanoparticles in chemical and biological sensing. *Chem. Rev.* **2012,** *112* (5), 2739-2779.
10. Schlücker, S., SERS microscopy: nanoparticle probes and biomedical applications. *ChemPhysChem* **2009,** *10* (9-10), 1344-1354.
11. Nie, S.; Emory, S. R., Probing single molecules and single nanoparticles by surface-enhanced Raman scattering. *science* **1997,** *275* (5303), 1102-1106.
12. Cialla, D.; März, A.; Böhme, R.; Theil, F.; Weber, K.; Schmitt, M.; Popp, J., Surface-enhanced Raman spectroscopy (SERS): progress and trends. *Anal. Bioanal. Chem.* **2012,** *403* (1), 27-54.
13. Le Ru, E.; Etchegoin, P., *Principles of Surface-Enhanced Raman Spectroscopy: and related plasmonic effects*. Elsevier: **2008**.
14. Guo, P.; Sikdar, D.; Huang, X.; Si, K. J.; Xiong, W.; Gong, S.; Yap, L. W.; Premaratne, M.; Cheng, W., Plasmonic core–shell nanoparticles for

SERS detection of the pesticide thiram: size-and shape-dependent Raman enhancement. *Nanoscale* **2015,** *7* (7), 2862-2868.
15. Jackson, J. B.; Halas, N. J., Surface-enhanced Raman scattering on tunable plasmonic nanoparticle substrates. *Proceedings of the National Academy of Sciences* **2004,** *101* (52), 17930-17935.
16. Samal, A. K.; Polavarapu, L.; Rodal-Cedeira, S.; Liz-Marzán, L. M.; Pérez-Juste, J.; Pastoriza-Santos, I., Size Tunable Au@ Ag core–shell nanoparticles: synthesis and surface-enhanced raman scattering properties. *Langmuir* **2013,** *29* (48), 15076-15082.
17. Yamamoto, Y. S.; Hasegawa, K.; Hasegawa, Y.; Takahashi, N.; Kitahama, Y.; Fukuoka, S.; Murase, N.; Baba, Y.; Ozaki, Y.; Itoh, T., Direct conversion of silver complexes to nanoscale hexagonal columns on a copper alloy for plasmonic applications. *Phys. Chem. Chem. Phys.* **2013,** *15* (35), 14611-14615.
18. Fan, W.; Lee, Y. H.; Pedireddy, S.; Zhang, Q.; Liu, T.; Ling, X. Y., Graphene oxide and shape-controlled silver nanoparticle hybrids for ultrasensitive single-particle surface-enhanced Raman scattering (SERS) sensing. *Nanoscale* **2014,** *6* (9), 4843-4851.
19. Shen, X. S.; Wang, G. Z.; Hong, X.; Zhu, W., Nanospheres of silver nanoparticles: agglomeration, surface morphology control and application as SERS substrates. *Phys. Chem. Chem. Phys.* **2009,** *11* (34), 7450-7454.
20. Lee, C. H.; Tian, L.; Singamaneni, S., Paper-based SERS swab for rapid trace detection on real-world surfaces. *ACS applied materials & interfaces* **2010,** *2* (12), 3429-3435.
21. Stamplecoskie, K. G.; Scaiano, J. C.; Tiwari, V. S.; Anis, H., Optimal size of silver nanoparticles for surface-enhanced Raman spectroscopy. *The Journal of Physical Chemistry C* **2011,** *115* (5), 1403-1409.
22. Albanese, A.; Tang, P. S.; Chan, W. C., The effect of nanoparticle size, shape, and surface chemistry on biological systems. *Annu. Rev. Biomed. Eng.* **2012,** *14*, 1-16.
23. Chithrani, B. D.; Ghazani, A. A.; Chan, W. C., Determining the size and shape dependence of gold nanoparticle uptake into mammalian cells. *Nano letters* **2006,** *6* (4), 662-668.
24. Ferguson, R. M.; Minard, K. R.; Krishnan, K. M., Optimization of nanoparticle core size for magnetic particle imaging. *J. Magn. Magn. Mater.* **2009,** *321* (10), 1548-1551.
25. Cole, J. R.; Halas, N., Optimized plasmonic nanoparticle distributions for solar spectrum harvesting. *Appl. Phys. Lett.* **2006,** *89* (15), 153120.
26. Wei, A.; Kim, B.; Sadtler, B.; Tripp, S. L., Tunable surface-enhanced Raman scattering from large gold nanoparticle arrays. *ChemPhysChem* **2001,** *2* (12), 743-745.

27. Njoki, P. N.; Lim, I.-I. S.; Mott, D.; Park, H.-Y.; Khan, B.; Mishra, S.; Sujakumar, R.; Luo, J.; Zhong, C.-J., Size correlation of optical and spectroscopic properties for gold nanoparticles. *The Journal of Physical Chemistry C* **2007,** *111* (40), 14664-14669.
28. Sant'Ana, A.; Rocha, T.; Santos, P.; Zanchet, D.; Temperini, M., Size-dependent SERS enhancement of colloidal silver nanoplates: the case of 2-amino-5-nitropyridine. *Journal of Raman Spectroscopy* **2009,** *40* (2), 183-190.
29. Lin, K.; Yi, J.; Hu, S.; Liu, B.-J.; Liu, J.-Y.; Wang, X.; Ren, B., Size Effect on SERS of Gold Nanorods Demonstrated via Single Nanoparticle Spectroscopy. *The Journal of Physical Chemistry C* **2016**.
30. Kang, H.; Yang, J.-K.; Noh, M. S.; Jo, A.; Jeong, S.; Lee, M.; Lee, S.; Chang, H.; Lee, H.; Jeon, S.-J., One-step synthesis of silver nanoshells with bumps for highly sensitive near-IR SERS nanoprobes. *Journal of Materials Chemistry B* **2014,** *2* (28), 4415-4421.
31. Liang, Z.; Susha, A. S.; Caruso, F., Metallodielectric Opals of Layer-by-Layer Processed Coated Colloids. *Adv. Mater.* **2002,** *14* (16), 1160-1164.
32. Talley, C. E.; Jackson, J. B.; Oubre, C.; Grady, N. K.; Hollars, C. W.; Lane, S. M.; Huser, T. R.; Nordlander, P.; Halas, N. J., Surface-enhanced Raman scattering from individual Au nanoparticles and nanoparticle dimer substrates. *Nano letters* **2005,** *5* (8), 1569-1574.
33. Wang, H.; Goodrich, G. P.; Tam, F.; Oubre, C.; Nordlander, P.; Halas, N. J., Controlled texturing modifies the surface topography and plasmonic properties of Au nanoshells. *The Journal of Physical Chemistry B* **2005,** *109* (22), 11083-11087.
34. Bagwe, R. P.; Yang, C.; Hilliard, L. R.; Tan, W., Optimization of dye-doped silica nanoparticles prepared using a reverse microemulsion method. *Langmuir* **2004,** *20* (19), 8336-8342.
35. Yao, L.; Xu, G.; Dou, W.; Bai, Y., The control of size and morphology of nanosized silica in Triton X-100 based reverse micelle. *Colloids and Surfaces A: Physicochemical and Engineering Aspects* **2008,** *316* (1), 8-14.
36. Stöber, W.; Fink, A.; Bohn, E., Controlled growth of monodisperse silica spheres in the micron size range. *J. Colloid Interface Sci.* **1968,** *26* (1), 62-69.
37. Yang, J.-K.; Kang, H.; Lee, H.; Jo, A.; Jeong, S.; Jeon, S.-J.; Kim, H.-I.; Lee, H.-Y.; Jeong, D. H.; Kim, J.-H., Single-Step and rapid growth of silver nanoshells as SERS-active nanostructures for label-free detection of pesticides. *ACS applied materials & interfaces* **2014,** *6* (15), 12541-12549.
38. Kobayashi, M.; Juillerat, F.; Galletto, P.; Bowen, P.; Borkovec, M., Aggregation and charging of colloidal silica particles: effect of particle size. *Langmuir* **2005,** *21* (13), 5761-5769.

39. Kang, H.; Yim, J.; Jeong, S.; Yang, J.-K.; Kyeong, S.; Jeon, S.-J.; Kim, J.; Eom, K. D.; Lee, H.; Kim, H.-I., Polymer-Mediated Formation and Assembly of Silver Nanoparticles on Silica Nanospheres for Sensitive Surface-Enhanced Raman Scattering Detection. *ACS applied materials & interfaces* **2013,** *5* (24), 12804-12810.
40. Kang, H.; Kang, T.; Kim, S.; Kim, J.-H.; Jun, B.-H.; Chae, J.; Park, J.; Jeong, D.-H.; Lee, Y.-S., Base Effects on Fabrication of Silver Nanoparticles Embedded Silica Nanocomposite for Surface-Enhanced Raman Scattering (SERS). *J. Nanosci. Nanotechnol.* **2011,** *11* (1), 579-583.
41. Link, S.; El-Sayed, M. A., Size and temperature dependence of the plasmon absorption of colloidal gold nanoparticles. *The Journal of Physical Chemistry B* **1999,** *103* (21), 4212-4217.
42. Fang, P. P.; Li, J. F.; Yang, Z. L.; Li, L. M.; Ren, B.; Tian, Z. Q., Optimization of SERS activities of gold nanoparticles and gold-core–palladium-shell nanoparticles by controlling size and shell thickness. *Journal of Raman Spectroscopy* **2008,** *39* (11), 1679-1687.
43. Schmidt, M. S.; Hübner, J.; Boisen, A., Large area fabrication of leaning silicon nanopillars for surface enhanced Raman spectroscopy. *Adv. Mater.* **2012,** *24* (10).
44. Deng, Y.-L.; Juang, Y.-J., Black silicon SERS substrate: effect of surface morphology on SERS detection and application of single algal cell analysis. *Biosens. Bioelectron.* **2014,** *53*, 37-42.
45. Baibarac, M.; Cochet, M.; Łapkowski, M.; Mihut, L.; Lefrant, S.; Baltog, I., SERS spectra of polyaniline thin films deposited on rough Ag, Au and Cu. Polymer film thickness and roughness parameter dependence of SERS spectra. *Synth. Met.* **1998,** *96* (1), 63-70.
46. Gersten, J. I., The effect of surface roughness on surface enhanced Raman scattering. *The Journal of Chemical Physics* **1980,** *72* (10), 5779-5780.
47. Gadelmawla, E.; Koura, M.; Maksoud, T.; Elewa, I.; Soliman, H., Roughness parameters. *J. Mater. Process. Technol.* **2002,** *123* (1), 133-145.
48. Rosales-Leal, J.; Rodríguez-Valverde, M.; Mazzaglia, G.; Ramon-Torregrosa, P.; Diaz-Rodriguez, L.; Garcia-Martinez, O.; Vallecillo-Capilla, M.; Ruiz, C.; Cabrerizo-Vilchez, M., Effect of roughness, wettability and morphology of engineered titanium surfaces on osteoblast-like cell adhesion. *Colloids and Surfaces A: Physicochemical and Engineering Aspects* **2010,** *365* (1), 222-229.
49. Ko, H.; Singamaneni, S.; Tsukruk, V. V., Nanostructured surfaces and assemblies as SERS media. *Small* **2008,** *4* (10), 1576-1599.
50. Li, L.; Hutter, T.; Steiner, U.; Mahajan, S., Single molecule SERS and detection of biomolecules with a single gold nanoparticle on a mirror junction. *Analyst* **2013,** *138* (16), 4574-4578.

51. Liu, H.; Zhang, L.; Lang, X.; Yamaguchi, Y.; Iwasaki, H.; Inouye, Y.; Xue, Q.; Chen, M., Single molecule detection from a large-scale SERS-active Au79Ag21 substrate. *Scientific Reports* **2011,** *1*.

국 문 초 록

표면 증강 라만 산란의 기판으로서 실리카 코어에 귀금속 껍질을 싼 나노 구조체는 실리카의 안정성이라는 장점으로 인해 많은 연구진에서 개발이 되어왔다. 하지만, 실리카 코어의 크기가 작아지게 되면 그러한 이점은 더 이상 효과적이지 않다. 본 연구에서는 코어 사이즈가 작아지면서 불안정성이 커져 합성 과정에서 뭉치는 문제를 극복함으로써 59, 82, 103, 124, 148 nm 크기에 해당하는 무정형의 실리카 나노 입자에 은 나노 껍질을 싼 나노 구조체를 합성하는 방법을 발표하였다. 작은 실리카 코어의 불안정성을 해결하기 위해 기존의 합성 방법에서 환원제, 분산제의 종류와 실리카 농도를 조절하였다.

우리는 그들의 사이즈에 따른 광학적 특성을 분석하기 위해 다른 사이즈의 은 껍질 범피 나노 구조체로부터 국소 표면 플라즈몬 공명과 표면 증강 라만 산란 스펙트럼을 측정하였다. 모든 사이즈의 은 껍질 범피 나노 구조체는 가시광선 영역에서 근 적외선 영역에 이르기까지 넓은 흡수 스펙트럼을 보여주었으며, 이는 결과적으로 3개의 다른 파장의 레이저에 대해 높은 라만 증강을 보여주게 된다.

우리는 은 껍질 범피 나노 구조체의 사이즈에 따른 라만 신호 세기의 경향성을 분석하는 데 있어서 라만 증강의 한 요인인 표면 거칠기 개념을 도입하였으며 표면 증강 라만 산란 현상과 거칠기 간의 상관 관계를 밝혀내었다. 따라서 이러한 결과는 추후 표면 증강 라만 산란 연구 목적에 따라 적절한 크기의 은 껍질 범피 나노 구조체를 선택하여 활용하는 데에 기초가 될 수 있고, 사이즈에 따른 표면 증강 라만 현상에 대해 명확한 이해를 제공할 수 있

다.

주요어 : 범피 실버 나노 쉘 (AgNS), 광학적 가변성, 국부 표면 플라즈몬 공명 (LSPR), 표면 증강 라만 산란 (SERS)

학번 : 2014-20960